A Critical Examination of Hypernova Remnant Candidates in M101. II. NGC 5471B

C.-H. Rosie Chen[1], You-Hua Chu[1], Robert Gruendl[1], and Shih-Ping Lai[2]

Department of Astronomy, University of Illinois, 1002 W. Green St., Urbana, IL 61801; c-chen@astro.uiuc.edu, chu@astro.uiuc.edu, gruendl@astro.uiuc.edu, slai@astro.uiuc.edu

and

Q. Daniel Wang

Department of Astronomy, University of Massachusetts, B-524 LGRT, Amherst, MA 01003; wqd@astro.umass.edu

ABSTRACT

NGC 5471B has been suggested to contain a hypernova remnant because of its extraordinarily bright X-ray emission. To assess its true nature, we have obtained high-resolution images in continuum bands and nebular lines with the *Hubble Space Telescope*, and high-dispersion long-slit spectra with the Kitt Peak National Observatory 4-m echelle spectrograph. The images reveal three supernova remnant (SNR) candidates in the giant H II region NGC 5471, with the brightest one being the 77×60 pc shell in NGC 5471B. The Hα velocity profile of NGC 5471B can be decomposed into a narrow component (FWHM = 41 km s^{-1}) from the background H II region and a broad component (FWHM = 148 km s^{-1}) from the SNR shell. Using the brightness ratio of the broad to narrow components and the Hα flux measured from the WFPC2 Hα image, we derive an Hα luminosity of $(1.4 \pm 0.1) \times 10^{39}$ ergs s^{-1} for the SNR shell. The [S II] λ6716/λ6731 doublet ratio of the broad velocity component is used to derive an electron density of ~ 700 cm^{-3} in the SNR shell. The mass of the SNR shell is thus 4600 ± 500 M$_\odot$. With a ~ 330 km s^{-1} expansion velocity implied by the extreme velocity extent of the broad component, the kinetic energy of the SNR

[1]Visiting astronomer, Kitt Peak National Observatory, National Optical Astronomy Observatories, operated by the Association of Universities for Research in Astronomy, Inc., under a cooperative agreement with the National Science Foundation.

[2]Current address: Jet Propulsion Lab, MS 169-506, 4800 Oak Grove Dr., Pasadena, CA 91109; slai@thisvi.jpl.nasa.gov

shell is determined to be 5×10^{51} ergs. This requires an explosion energy greater than 10^{52} ergs, which can be provided by one hypernova or multiple supernovae. Comparing to SNRs in nearby active star formation regions, the SNR shell in NGC 5471B appears truly unique and energetic. We conclude that the optical observations support the existence of a hypernova remnant in NGC 5471B.

Subject headings: galaxies: individual (M101) – H II regions – ISM: bubbles – ISM: kinematics and dynamics – supernova remnants – X-rays: ISM

1. Introduction

Two supernova remnants (SNRs), MF 83 (Matonick & Fesen 1997) and NGC 5471B (Skillman 1985), in the giant spiral galaxy M101 have been recently suggested to be candidates for "hypernova remnants" (Wang 1999), because their explosion energies appear to be 1–2 orders of magnitude higher than the canonical 10^{51} ergs explosion energy for normal SNRs (Jones et al. 1998). Such high explosion energies are rivaled only by the "hypernovae" proposed by Paczyński (1998) and Fryer & Woosley (1998) to explain the gamma-ray bursts (GRBs). As the explosion energies of MF 83 and NGC 5471B were derived from their X-ray luminosities measured from *ROSAT* observations which did not resolve these sources spatially, it is of interest to investigate the nature of these two hypernova remnant candidates at optical wavelengths with high angular and spectral resolutions.

The analysis of optical and X-ray observations of MF 83 has been reported by Lai et al. (2001, hereafter Paper I). It is shown that MF 83 is a superbubble around an OB association in which multiple supernova explosions are likely to have taken place. Optical observations do not provide compelling evidence for a single, super-energetic supernova explosion. Furthermore, *Chandra* X-ray observation of M101 shows that MF 83 is dominated by a variable point source (Snowden et al. 2001). Therefore, it is unlikely that MF 83 is a hypernova remnant.

The hypernova remnant candidate NGC 5471B was initially identified and confirmed as an SNR in the B-component of the giant H II region NGC 5471 (hence the name NGC 5471B) by Skillman (1985) based on its nonthermal radio emission and high [S II]/Hα ratio. The shocked, high-velocity gas in NGC 5471B was detected by Chu & Kennicutt (1986), who concluded that the SNR was supermassive. The X-ray emission from the giant H II region NGC 5471 was reported by Williams & Chu (1995), but the association of X-ray emission with the SNR per se was made by Wang (1999).

NGC 5471B is an unusual SNR in an active star formation region. To study the giant H II

region NGC 5471 and the SNR NGC 5471B, we have obtained *Hubble Space Telescope (HST)* Wide Field and Planetary Camera 2 (WFPC2) images of NGC 5471 in emission lines and continuum bands. These images are used to search for SNR candidates in NGC 5471, and to examine the physical structure and stellar/interstellar environment of the SNR NGC 5471B. We have also obtained new echelle spectra of NGC 5471B with the 4 m telescope at Kitt Peak National Observatory (KPNO) in order to kinematically separate the SNR from the background H II region. This paper reports these observations (§2), the SNR candidates identified in NGC 5471 (§3), a detailed analysis of the physical properties of NGC 5471B (§4), and a discussion of the nature of NGC 5471B as a hypernova remnant (§5).

2. Observations & Data Reduction

2.1. *HST* WFPC2 Images

The *HST* WFPC2 images of NGC 5471 were obtained on 1997 November 1 for the Cycle 6 program GO-6928. The observations were made through two emission-line filters, *F656N* (Hα) and *F673N* ([S II]), and two continuum filters, *F547M* (Strömgren y) and *F675W* (WFPC2 R) (Biretta et al. 1996). The journal of observations is given in Table 1.

The calibrated WFPC2 images, produced by the standard *HST* pipeline processes, were further reduced with the IRAF and STSDAS routines. The images were all corrected for the intensity- and position-dependent charge transfer efficiency (CTE) by applying a linear ramp with a correction factor chosen according to the average counts of the sky background (Holtzman et al. 1995). The images taken with the same filter were then combined to remove cosmic rays and to produce a total-exposure map.

To extract the Hα and [S II] line fluxes from the emission line images, it is necessary to subtract the continuum emission. As the giant H II region NGC 5471 is very luminous, its Hα emission contributes significantly to the broad R-band (*F675W*) image. Therefore, we first subtracted a scaled Hα image from the *F675W* image, then scaled the resultant image and subtracted it from the line images. The scaling took into account the exposure times and the filter transmission curves (Biretta et al. 1996).

The continuum-subtracted Hα and [S II] images were processed with the standard procedures (Chen et al. 2000) to extract line fluxes and to produce the [S II]/Hα ratio map. Due to the ~ 300 km s^{-1} redshift of M101, two corrections have been applied to the extracted Hα flux. First, as the filter transmission of the red-shifted Hα line is $\sim 93\%$ of the peak transmission, the extracted Hα flux is multiplied by a correction factor of 1.07. Second, the [N II] λ6548 line is red-shifted into the Hα bandpass at $\sim 91\%$ of the peak transmission. Adopting

the de-reddened [N II] λ6548+6584/Hβ ratio of 0.23 and the logarithmic extinction at Hβ, c(Hβ), of 0.23 for NGC 5471B reported by Kennicutt & Garnett (1996), we find that the [N II] λ6548 line contributes to $\sim$ 2% of the total transmitted flux; therefore, an additional correction factor of 0.98 is applied to the extracted Hα flux.

To suppress artificial fluctuations in the [S II]/Hα ratio in regions where the nebular emission is faint (and hence noisy), we have clipped pixels with fluxes less than 3σ above the sky background for both the Hα and [S II] images of NGC 5471. The Hα, *F675W*, *F547M*, continuum-subtracted Hα, continuum-subtracted [S II], and [S II]/Hα images of NGC 5471 are presented in Figure 1. The A–E components of NGC 5471 defined by Skillman (1985) are marked in Fig. 1a, and the [S II]-bright shells are marked in Fig. 1f. Corresponding close-up images of NGC 5471B are shown in Figure 2.

Stellar photometry was carried out using the APPHOT package in IRAF for the *F547M* and *F675W* images of NGC 5471B. Because of the complexity in the stellar field, we manually selected stellar sources in NGC 5471B and its surroundings and derived their apparent magnitudes, m_{F547M} and m_{F675W}. The uncertainties in the photometric measurements formally given by APPHOT are 0.1–0.2 mag. In most cases the true errors must be larger, if the uncertainties in aperture correction and sky background are included. The photometric uncertainties are generally larger in m_{F675W} than in m_{F547M}, because the nebular emission produces rapid variations in the background in the *F675W* image. Varying the background aperture may result in changes in m_{F675W} by $\sim$ 0.2 mag for most stars, and up to $\sim$ 0.5 mag for stars near bright nebulosities. To reduce the errors introduced by the nebular contamination in the *F675W* band, we have also carried out stellar photometry for the Hα-subtracted *F675W* image, and designated this apparent magnitude as $m_{F675W'}$. Table 2 lists the resulting magnitudes and colors of the stellar sources in NGC 5471B. The stellar sources are marked on the *F547M* image in Figure 3a, and the Hα-subtracted *F657W* image is shown in Fig. 3b.

2.2. KPNO 4 m Echelle Observations

High-dispersion spectra of NGC 5471 were obtained with the echelle spectrograph on the KPNO 4 m telescope on 1999 June 30 and July 1. The observations were made with the 79-63 echelle grating and the 226-1 cross disperser. The 2048 $\times$ 2048 T2KB CCD detector was used to record the spectra. The pixel size is 24 μm. To reduce the readout noise, the data were read out with the pixels binned by a factor of 2 in the spatial direction. The final data array thus has a scale of $0\farcs57$ pixel^{-1} along the slit, and $\sim$ 0.08Å pixel^{-1} along the dispersion.

Two slit positions were observed, one centered on the hypernova remnant candidate NGC 5471B (= Shell 1 in Fig. 1f) and the other on a [S II]-bright shell to its north (Shell 2 in Fig. 1f). For both observations, the slit was E-W oriented with a slitwidth large enough to cover the entire shell, 2.″0 for NGC 5471B and 1.″5 for Shell 2. NGC 5471B was observed with a total exposure time of 30 min, while Shell 2 only 10 min. The exact slit positions, shown in Fig. 2a, were recovered by matching the surface brightness profiles along the slits to those extracted from the WFPC2 Hα image. The accuracy of the position matching is better than 0.″5. The instrumental FWHM, determined from Gaussian fits to the unresolved telluric lines, is 16.8 ± 0.5 km s^{-1} for NGC 5471B, and 12.8 ± 0.5 km s^{-1} for Shell 2.

The Hα+[N II] echellograms of NGC 5471B and Shell 2 and the [S II] $\lambda\lambda$6716, 6731 echellogram of NGC 5471B are displayed in Figure 4. These new echelle data reveal high-velocity gas over a larger velocity range than that reported by Chu & Kennicutt (1986) because of an improvement in the S/N of data.

The IRAF software was used for data reduction and analysis. We followed the same reduction procedures as described in Paper I. The sky-subtraction is more difficult for NGC 5471B, because it is embedded in the giant H II region NGC 5471, and the nebular emission fills the entire length of the slit. We have thus adopted the sky spectrum extracted from the observations of MF 83 reported in Paper I to remove the telluric lines in the spectrum of NGC 5471B. The results are satisfactory, because MF 83 is sufficiently close to NGC 5471B and the observations of MF 83 were made immediately after those of NGC 5471B. The sky-subtracted Hα line profile of NGC 5471B extracted over 2.″9 along the slit is Hanning smoothed over five adjacent pixels and displayed in Figure 5.

3. Supernova Remnant Candidates in NGC 5471

SNRs are commonly diagnosed by their high [S II]/Hα ratios, as S^+ can be collisionally excited in the cooling region behind SNR shocks and emit strongly in the [S II] $\lambda\lambda$6716, 6731 lines (Raymond 1979). Although the [S II]/Hα ratios of known SNRs are frequently observed to be 0.5–1.0 (Fesen, Blair, & Kirshner 1985), optical SNR surveys have used a lower threshold, 0.4–0.45, to identify SNR candidates because nebular backgrounds tend to lower the apparent [S II]/Hα ratios (e.g., Long et al. 1990; Matonick & Fesen 1997).

The [S II]/Hα ratio map of NGC 5471 (Fig. 1f) shows three shells with enhanced [S II] emission. The positions, sizes, and [S II]/Hα ratios of these three shells are listed in Table 3. The apparent [S II]/Hα ratios of these shells, 0.2–0.4, are higher than those of the background H II region, $\sim$ 0.1, but lower than the SNR identification threshold. These low observed

ratios are not surprising, given that the background H II region is extremely bright. We have measured the average background emission from regions around the shells and subtracted the background from the [S II] and Hα images. The background-subtracted [S II]/Hα ratios of the [S II]-bright shells, also given in Table 3, are in the range 0.5–0.8, fully consistent with those of SNRs.

The [S II]-bright shells in NGC 5471 have sizes of 50–80 pc, for a distance of 7.2 Mpc to M101 (Stetson et al. 1998). Interstellar shells with these large sizes and high [S II]/Hα ratios can be either classical SNRs or superbubbles (Lasker 1977). To distinguish between these two possibilities, the stellar content and nebular dynamics need to be examined.[3] A shell is likely to be a superbubble, if it encompasses a high concentration of blue stars and the shell has an expansion velocity $\ll 100$ km s^{-1}. Conversely, the existence of SNRs can be inferred, if no concentrations of blue stars are present or the shell expansion velocity is high, $\gg 100$ km s^{-1}.

Shell 1, the brightest of the three [S II]-enhanced shells in NGC 5471, corresponds to the SNR NGC 5471B. The *HST* WFPC2 images in Fig. 2 show concentrations of blue stars within the boundary of Shell 1, making the existence of a superbubble a distinct possibility. On the other hand, the echelle spectrum of Shell 1 (Fig. 5) shows high-velocity gas over a velocity range of ~ 620 km s^{-1}, which has been seen only in SNRs. It is thus most likely that Shell 1 contains a SNR but the physical conditions are complicated by the complex stellar environment. A detailed analysis of Shell 1 will be presented in §4.

Shell 2 is at $\sim 2''$ north of NGC 5471B. With a size of 52×50 pc, it is the smallest of the three shells. It exhibits a clear ring morphology in both the Hα and [S II] lines. The *F547M* continuum image (Fig. 2c) shows sparse distribution of stars in the vicinity of Shell 2 with no specific concentrations within the shell interior. The echellogram of Shell 2 (Fig. 4c) shows a very broad Hα line with high-velocity gas detected over a velocity range of ~ 450 km s^{-1}. The lack of prominent concentrations of stars and the large expansion velocity in the high-velocity gas both support the existence of a SNR. Even if Shell 2 is a superbubble formed by a small OB association, it must have been recently accelerated by a SNR.

Shell 3 is located at the low-density outskirts of NGC 5471. Its size, ~ 70 pc, is comparable to that of Shell 1. It has the highest [S II]/Hα ratios among the three [S II]-bright shells, and its background-subtracted [S II]/Hα ratio is within the higher range of SNRs. The *F547M* continuum image (Fig. 1c) does not detect any bright stars or concentrations of

[3]The conventional SNR diagnostics, bright X-ray emission and nonthermal radio emission, are ineffective for SNRs in bright giant H II regions such as NGC 5471 because shocked fast stellar winds can produce X-ray emission and the thermal emission from the H II region overwhelms the nonthermal emission from SNRs.

stars in the interior or along the rim of Shell 3. It is unlikely that Shell 3 is a superbubble. Although no kinematic information is available for Shell 3 and the size of Shell 3 is larger than the average size of Galactic SNRs, we consider that Shell 3 is probably a bona fide SNR and its large size is a direct consequence of the low density in its interstellar environment.

4. Analysis of Physical Properties of NGC 5471B

4.1. Interstellar and Stellar Environment of NGC 5471B

As shown in Fig. 1, NGC 5471B has a complex environment. It is not trivial to separate the SNR from the background. Different morphologies are seen in the Hα and [S II] images. Since SNR shocks can be diagnosed by high [S II]/Hα ratios, the [S II] image should illustrate more clearly the boundary of the SNR. Indeed, the continuum-subtracted [S II] image provides the most well-defined limb-brightened shell morphology of NGC 5471B. The shell is elongated with a size of $2\farcs2 \times 1\farcs7$, or 77×60 pc. A bright emission patch is present in the southwest corner. Along this direction, [S II]-bright emission is still present exterior to the shell, making the SNR boundary somewhat ambiguous. Owing to this patch of [S II]-bright emission, the [S II]/Hα ratio map in Fig. 2f shows high ratios over a region $\sim 50\%$ larger than the [S II] shell. We will assume that the limb-brightened [S II] shell represents the SNR in NGC 5471B.

The continuum-subtracted Hα image shows an oval disk of emission with a slight limb-brightening at the west rim and a bright compact emission region at the southeast corner. This bright compact region, showing bright stellar emission in the continuum bands and having the lowest [S II]/Hα ratio, is most likely a high-excitation H II region. The oval disk of Hα emission, roughly coincident with the [S II] shell, is probably associated with the SNR. The SNR is superposed on a bright H II background; the average surface brightness at the main body of the SNR is only 2-4 times as bright as those of the surrounding regions.

The *F547M* image shows many concentrations of stars in and around NGC 5471B. Within the main body of NGC 5471B, two peaks of stellar emission are present at the eastern end. The brighter stellar source is coincident with the aforementioned bright high-excitation H II region; the fainter stellar source is not associated with prominent Hα emission, but the [S II]/Hα ratio in its vicinity is low, indicating that it is also inside an H II region. There is diffuse continuum emission along and interior to the south rim of the main body. Since the *F547M* band does not contain any bright nebular emission lines and the distribution of this continuum light is different from that of the Hα emission, this diffuse continuum emission most likely originates from an extended distribution of unresolved stars similar to the "star

clouds" defined by Lucke & Hodge (1970) for OB associations in the Large Magellanic Cloud (LMC).

Many peaks of stellar continuum emission are present in the vicinity of NGC 5471B (see Fig. 3). Their brightnesses in the *F547M*, *F675W*, and Hα-subtracted *F675W* bands (m_{F547M}, m_{F675W}, and $m_{F675W'}$) are given in Table 2. To determine the nature of these stellar sources, we present in Figure 6 a color-magnitude diagram of these sources using m_{F547M} and $m_{F675W'}$. To facilitate comparisons with normal stars, we have synthesized m_{F547M} and m_{F675W} for stars of different spectral types and luminosity classes using the Kurucz (1993) stellar atmosphere models and the WFPC2 filter transmission curves (Biretta et al. 1996). The synthetic photometry was calculated for a metallicity of 1/10 $Z_{\odot}$, a reddening of $E(B-V) = 0.16$ mag (Kennicutt & Garnett 1996), and a distance modulus of 29.3 mag (= 7.2 Mpc, Stetson et al. 1998). In Fig. 6, the synthetic main sequence from O3 V downward is plotted in a thick line and the supergiants in a thin line with spectral types marked. It is immediately clear from the comparison that all identified stellar sources are either supergiants or composite with multiple stars.

While the brightest stellar source, #18, is outside and to the south of the shell in NGC 5471B, the next two brightest sources, #21 and #22, are the two stellar concentrations inside the shell. All these three bright sources have blue colors, and must be OB associations or clusters. Source #18, not surrounded by a recognizable H II region, must be the oldest among these three sources. It is thus apparent that the SNR shell in NGC 5471B encompasses two young OB associations.

4.2. Luminosity and Dynamics of the SNR Shell in NGC 5471B

Several physical properties of the SNR shell in NGC 5471B can be derived from the multi-order echelle observations. First of all, the expansion of the shell can be determined from the Hα line profile. The echelle image of the Hα and [N II] lines of NGC 5471B (Fig. 4) shows narrow cores and extended wings superposed on a faint stellar continuum. The presence of the extended wings in the [N II] lines indicates that this component originates from shocked gas, as opposed to stellar atmospheric emission from Wolf-Rayet (WR) stars or luminous blue variables (LBVs). The Hα velocity profile of NGC 5471B (Fig. 5), extracted over 2.″9 along the 2″-wide slit, can be fitted by a narrow component of FWHM = 41 ± 2 km s^{-1} and a broad component of FWHM = 148 ± 5 km s^{-1}. The widths of the narrow and broad components are in the ranges typical for H II regions and SNRs, respectively (Chu & Kennicutt 1988, 1994b). Therefore, we assign the narrow component to the background H II region and the broad component to the SNR.

The decomposition of SNR and H II region components within the echelle aperture allows us to determine the Hα luminosity of the SNR from the *HST* WFPC2 Hα image of NGC 5471B. The total Hα flux within the $2'' \times 2''.9$ aperture centered on the SNR shell is $(2.6 \pm 0.2) \times 10^{-13}$ ergs cm^{-2} s^{-1}. The error originates mostly from the imprecise aperture of the echelle observation which is affected by the seeing. The best spectral fit to the Hα velocity profile indicates that the broad component is 1.4 times as bright as the narrow component. Therefore, the Hα flux from the SNR is $(1.5 \pm 0.1) \times 10^{-13}$ ergs cm^{-2} s^{-1}. This flux is consistent with the value 1.5×10^{-13} ergs cm^{-2} s^{-1} estimated by Chu & Kennicutt (1986). For a distance of 7.2 Mpc and a c(Hβ) of 0.23 (Kennicutt & Garnett 1996), the Hα luminosity of the SNR is $(1.4 \pm 0.1) \times 10^{39}$ ergs s^{-1}.

The mass of the SNR can be derived from its Hα luminosity and density. Our echelle observation detected the [S II] $\lambda\lambda$6716, 6731 doublet. The velocity profiles of the [S II] doublets are likewise fitted by narrow and broad components. The [S II] λ6716/λ6731 ratio is 1.4 and 1.0 for the narrow and broad components, respectively. The [S II] doublet ratio for the narrow component is at the low-density limit, implying that the electron density of the H II region is $\ll 50$ cm^{-3}. The [S II] doublet ratio for the broad component, on the other hand, corresponds to an electron density of ~ 700 cm^{-3}, adopting an electron temperature of 13,000 K (Skillman 1985). This density and the above-derived Hα luminosity infer a mass of 4600 ± 500 M$_\odot$ in the SNR shell. This mass is consistent with but more accurate than the value 6500 ± 3000 M$_\odot$ estimated by Chu & Kennicutt (1986) because of the updated atomic constants and more direct measurement of the electron density used in our current work.

Finally, the kinetic energy of the SNR shell can be estimated from the mass and expansion velocity. The expansion velocity of the SNR cannot be measured directly because the SNR is not spatially resolved in the echelle data. As the integrated velocity profile of the SNR is weighted by the surface brightness of each emission region within the SNR, the FWHM of the integrated profile cannot be used to determine the expansion velocity of the SNR. Instead, we adopt the observed extreme velocity offsets of the broad line as a lower limit of the expansion velocity of the SNR. The approaching and receding sides of the SNR are detected up to about -290 km s^{-1} and $+330$ km s^{-1} with respect to the systemic velocity of the H II region, respectively (see Fig. 5). Thus we adopt an expansion velocity of 330 km s^{-1} for the SNR, and the kinetic energy of the SNR is 5.0×10^{51} ergs. The kinetic energy estimated by Chu & Kennicutt (1986) is 20 times smaller because they used too small an expansion velocity for the SNR.

4.3. X-ray Emission and Hot Ionized Gas of NGC 5471B

X-ray emission from NGC 5471 has been detected by *ROSAT* observations with both the Position Sensitive Proportional Counter (PSPC) and the High-Resolution Imager (HRI). The angular resolutions of the PSPC and HRI were not adequate to distinguish between point sources and diffuse emission from NGC 5471; however, the spectral shape of the PSPC spectrum of NGC 5471 is consistent with that of thin plasma emission (Williams & Chu 1995). Using an ultradeep, 227 ks, *ROSAT* HRI image of M101, Wang, Immler, & Pietsch (1999) detected NGC 5471 at a count rate of 1.22 counts ks^{-1}, corresponding to an X-ray luminosity of 3×10^{38} ergs s^{-1} (Wang 1999).

We have plotted the X-ray contours extracted from the 227 ks *ROSAT* HRI image over the *HST* WFPC2 [S II] image of NGC 5471 in Figure 7. The X-ray contours are centered near NGC 5471B. Given the combined pointing errors of the *HST* and *ROSAT*, a few arcsec, it is very likely that the X-ray source is centered at NGC 5471B. The high-resolution *Chandra* observation of NGC 5471 (scheduled for Cycle 3) will be able to determine unambiguously the position and spatial extent of this X-ray emission.

Wang (1999) used the observed X-ray emission from NGC 5471 in conjunction with the Sedov solution for a SNR, and computed a thermal energy of $\sim 10^{52}$ ergs for the hot gas in the NGC 5471B SNR. This amount of thermal energy is about twice as high as the kinetic energy we have derived for the 10^4 K ionized expanding shell of this SNR.

5. Discussion

The term "hypernova" has been vaguely used in theoretical contexts until recently when the connection between GRBs and supernovae was illustrated observationally through SN 1988bw (Kulkarni et al. 1998) and SN 1997cy (Germany et al. 2000). Analyses of the light curves and spectral variations of these two supernovae indicate that the kinetic energy released in the supernova explosion was $3-5 \times 10^{52}$ ergs (Nakamura et al. 2001; Turatto et al. 2000). Such explosion energies are more than an order of magnitude higher than the canonical supernova explosion energy of 10^{51} ergs, qualifying these supernovae as "hypernovae". Hypernovae without GRB counterparts have also been reported, e.g., SN 1997ef (Mazzali, Iwamoto, & Nomoto 2000). Thus, we consider a supernova with an explosion energy greater than 10^{52} ergs as a hypernova, and a SNR that requires such a high explosion energy as a hypernova remnant.

The SNR in NGC 5471B has been suggested to be a hypernova remnant because its X-ray emission implies a thermal energy that requires a supernova explosion energy greater

than 10^{52} ergs (Wang 1999). Our high-resolution imaging and spectroscopic observations at optical wavelengths have allowed us to (1) resolve the shell structure of the SNR, (2) examine the stellar and interstellar environments of the SNR, (3) study the expansion dynamics of the SNR, (4) separate the Hα flux of the SNR from the background H II region emission, and (5) determine the mass and kinetic energy of the SNR shell. Using these results we are now able to critically examine the nature of the hypernova remnant candidate NGC 5471B.

5.1. Explosion Energy Requirement of the SNR Shell in NGC 5471B

NGC 5471B possesses typical signatures of SNRs, e.g., nonthermal radio emission, high [S II]/Hα ratio, and X-ray spectrum consistent with those of thin plasma emission (Skillman 1985; Williams & Chu 1995). It is most certain that NGC 5471B contains a SNR. The *HST* WFPC2 images of NGC 5471B show a dominant, [S II]-bright 77 × 60 pc shell, which is responsible for the enhanced [S II]/Hα ratio. The echelle observations of NGC 5471B have established that there is a broad velocity component associated with high-velocity shocks. From the comparison between the [S II] and Hα velocity profiles of NGC 5471B (Fig. 4), it is clear that the broad velocity component is responsible for the [S II]-enhancement. Therefore, the [S II]-bright shell shown in the WFPC2 images must produce the broad velocity component in the echelle spectra.

We can further confirm that the [S II]-bright shell corresponds to the broad velocity component using a consideration of the brightnesses of the shell and the background H II region. The Hα velocity profile shows that the broad component contributes to 1.4/(1+1.4) = 58% of the total Hα flux within the $2''$ × $2''.9$ echelle aperture. Using the WFPC2 Hα image and assuming that the shell is superposed on an H II region with an average surface brightness similar to that of the surrounding regions, we find that the shell contributes to ∼ 54% of the total Hα flux within a $2''$ × $2''.9$ aperture centered on the shell. The similarity in the shell's and the broad component's contributions to the total flux within the same aperture strengthens the conclusion that the [S II]-bright shell gives rise to the broad velocity component. The shell expansion velocity, ∼ 330 km s^{-1}, is higher than those of most SNRs in the LMC (Chu & Kennicutt 1988), and certainly can produce the radio and X-ray signatures of SNRs by shocks[4]. Therefore, we believe that all observed SNR signatures originate from this [S II]-bright shell, and will identify this shell as the SNR.

[4]Note that the shock velocities are higher than the observed expansion velocity of the optical SNR shell. For example, the velocity of an adiabatic shock is 4/3 times the shell expansion velocity. Furthermore, the optically detected material is likely associated with SNR shocks propagating through dense clouds, while the shocks in the intercloud medium are faster but their post-shock material is too tenuous to be detected.

As we have derived in §4.2, the expanding SNR shell in NGC 5471B has a mass of 4,600 $M_\odot$ and a kinetic energy of 5.0×10^{51} ergs. The kinetic energy in a mature SNR shell is much lower than 30% of the supernova explosion energy (Chevalier 1974); thus the observed kinetic energy in the SNR shell in NGC 5471B requires an explosion energy greater than 10^{52} ergs. Moreover, Wang (1999) assumed that the X-ray emission from NGC 5471B originates from the hot shocked gas in a SNR, and derived a thermal energy of $\sim 10^{52}$ ergs for the SNR. Both the optical and X-ray considerations require a supernova explosion energy $> 10^{52}$ ergs; therefore, the [S II]-bright expanding shell in NGC 5471B must be a hypernova remnant or energized by a burst of multiple supernova explosions.

5.2. Comparison with Other SNRs in Nearby Star Formation Regions

Was the [S II]-bright shell in NGC 5471B produced by a single hypernova explosion? It is almost impossible to answer this question, especially since the shell is in an active star formation region with two prominent OB associations (see Figs. 3 & 6) projected within the shell, as described in §4.1. It is nevertheless possible to compare NGC 5471B to other SNRs in nearby active star formation regions in order to determine whether the shell in NGC 5471B is a common entity. We will use the sample of star formation regions in the LMC and NGC 604 in M33 for comparison.

Convincing SNR signatures have been detected in at least 13 OB associations in the LMC (Chu 1997). Of these, eight contain SNRs showing signatures at all wavelengths, and all of them are in the outskirts of their associated OB associations. The other five contain SNRs within their superbubbles and show only X-ray signatures. These superbubbles have sizes 50–100 pc, comparable to that of the shell in NGC 5471B; however, their expansion velocities are $\ll 100$ km s^{-1}, much slower than that of the NGC 5471B shell. The shell in NGC 5471B is much more energetic than the normal superbubbles around OB associations.

We may further dismiss the two prominent OB associations projected within the shell of NGC 5471B as the providers of multiple supernovae. The existence of bright compact H II regions around these OB associations indicate that they are young and the surrounding interstellar gas has not been dispersed by SNR shocks. It is thus unlikely that the two OB associations in the NGC 5471B shell energized the SNR shell. Moreover, the size and expansion velocity of the SNR shell implies an upper limit of 1×10^5 yr for the dynamic age. In order to have more than 10 normal supernovae from an OB association within such a small time span, these supernovae must have the shortest-lived progenitors, i.e., the most massive stars. Assuming that all 10 progenitors were O3 V stars with initial masses of 100–120 $M_\odot$ and adopting Salpeter's (1955) slope for the initial mass function, we expect the

OB associations to contain 250 stars in the mass range of 25–100 $M_\odot$, corresponding to the later-type O stars (Schaerer & de Koter 1997). The m_{F547M} magnitudes of the two OB associations projected within the NGC 5471B shell are equivalent to 70 and 45 O6 V stars for sources #21 and #22, respectively. The total number of O stars in these two OB associations is most likely smaller than 115 because some of the stars may be supergiants that are several times brighter than their main-sequence counterparts. Therefore, the expected number of O stars exceeds the total number of O stars implied by m_{F547M} by more than a factor of 2. Thus, the observed OB associations in the shell of NGC 5471B are unable to produce enough supernovae within the dynamic age and power the shell.

It would be appropriate to compare NGC 5471B to the giant H II region 30 Doradus in the LMC, as 30 Dor is the most active star formation and has the highest concentration of massive stars in the LMC. Figure 8 displays NGC 5471B and 30 Dor at the same physical scale over an area of 200 pc × 200 pc, adopting a distance of 50 kpc to the LMC (Feast 1999). Within this region, the Hα luminosity of NGC 5471B is 4.6×10^{39} ergs s^{-1}, and 30 Dor 6.2×10^{39} ergs s^{-1} (Kennicutt & Hodge 1986; Mathis, Chu, & Peterson 1985). The similarity in the Hα luminosity implies a similarity in the ionizing power of stars encompassed in these two regions. It would then be truly a fair comparison between NGC 5471B and 30 Dor.

Despite the similarity in ionizing power, the nebular structure of NGC 5471B is very different from 30 Dor. NGC 5471B is dominated by the SNR shell, while 30 Dor is dominated by several shell structures of comparable sizes. The kinematic structure of 30 Dor has been mapped in great detail by Chu & Kennicutt (1994a). The central shell around the R136 cluster in 30 Dor is much smaller (30 pc in diameter) and expands much more slowly ($\sim$ 130 km s^{-1}) than the shell in NGC 5471B. The five largest shells in 30 Dor, designated as Shells 1–5 by Wang & Helfand (1991), show a common kinematic structure: a slowly expanding shell with $V_{exp} \ll 100$ km s^{-1} superposed by additional shocked clouds with velocity offsets up to $\pm$300 km s^{-1}. The Hα fluxes from these shells in 30 Dor are dominated by the slow expanding shell component. We use Shell 1 in 30 Dor as an example. The echelle observations along four slit positions in 30 Dor-Shell 1, marked in Fig. 8, are used to simulate an integrated Hα velocity profile of 30 Dor-Shell 1, shown in Figure 9. The "pseudo-integrated" profile of 30 Dor-Shell 1 shows a narrow core and broad wings, but the broad wings are highly asymmetric and the broad component contributes to only 22% of the total flux.

The fast expanding shell in NGC 5471B is unmatched by any comparable shells in the LMC. The giant H II region NGC 604 in M33 has also been studied in detail with similar echelle observations (Yang et al. 1996). Its kinematic structure is very similar to that of 30 Dor, and it does not have any shell with an expansion velocity or luminosity matching those of the shell in NGC 5471B. Therefore, it becomes clear that the fast expanding shell in

NGC 5471B is truly outstanding and unique. It could not have been produced by multiple supernovae as in the giant H II regions 30 Dor and NGC 604. Therefore, we conclude that it is very likely that the energetic SNR in NGC 5471B was produced by a hypernova.

This research is supported by the NASA grant STI6829.01-95A.

REFERENCES

Biretta, J. A., et al. 1996, WFPC2 Instrument Handbook, Version 4.0 (Baltimore: STScI)

Chen, C.-H. R., Chu, Y.-H., Gruendl, R. A., & Points, S. D. 2000, AJ, 119, 1317

Chevalier, R. A. 1974, ApJ, 188, 501

Chu, Y.-H. 1997, AJ, 113, 1815

Chu, Y.-H., & Kennicutt, R. C., Jr. 1986, ApJ, 311, 85

Chu, Y.-H., & Kennicutt, R. C., Jr. 1988, AJ, 95, 1111

Chu, Y.-H., & Kennicutt, R. C., Jr. 1994a, ApJ, 425, 720

Chu, Y.-H., & Kennicutt, R. C., Jr. 1994b, ApSS, 216, 253

Feast, M. 1999, IAU Symp. 190: New Views of the Magellanic Clouds, 190, 542

Fesen, R. A., Blair, W. P., & Kirshner, R. P. 1985, ApJ, 292, 29

Fryer, C., & Woosley, S. 1998, ApJ, 502, 9

Germany, L. M., Reiss, D. J., Sadler, E. M., Schmidt, B. P., & Stubbs, C. W. 2000, ApJ, 533, 320

Holtzman, J. A., et al. 1995, PASP, 107, 1065

Jones, T. W., et al. 1998, PASP, 110, 125

Kennicutt, R. C., & Garnett, D. R. 1996, ApJ, 456, 504

Kennicutt, R. C., & Hodge, P. 1986, ApJ, 306, 130

Kulkarni, S. R. et al. 1998, Nature, 395, 663

Kurucz, R. 1993, ATLAS9 Stellar Atmosphere Programs and 2 km/s grid. Kurucz CD-ROM No. 13. Cambridge, Mass.: Smithsonian Astrophysical Observatory, 1993., 13

Lai, S.-P., Chu, Y.-H., Chen, C.-H. R., Ciardullo, R., & Grebel, E. K. 2001, ApJ, 547, 754 (Paper I)

Lasker, B. M. 1977, ApJ, 212, 390

Long, K. S., Blair, W. P., Kirshner, R. P., & Winkler, P. F. 1990, ApJS, 72, 61

Lucke, P. B., & Hodge, P. W. 1970, AJ, 75, 171

Mathis, J. S., Chu, Y.-H., & Peterson, D. E. 1985, ApJ, 292, 155

Matonick, D. M., & Fesen, R. A. 1997, ApJS, 112, 49

Mazzali, P. A., Iwamoto, K., & Nomoto, K. 2000, ApJ, 545, 407

Nakamura, T., Mazzali, P. A., Nomoto, K., & Iwamoto, K. 2001, ApJ, 550, 991

Paczyński, B. 1998, ApJ, 494, 45

Raymond, J. C. 1979, ApJS, 39, 1

Salpeter, E. E. 1955, ApJ, 121, 161

Schaerer, D., & de Koter, A. 1997, A&A, 322, 598

Skillman, E. D. 1985, ApJ, 290, 449

Snowden, S. L., Mukai, K., Pence, W., & Kuntz, K. D. 2001, AJ, 121, 3001

Stetson, P. B., et al. 1998, ApJ, 508, 491

Turatto, M. et al. 2000, ApJ, 534, L57

Wang, Q. D. 1999, ApJ, 517, L27

Wang, Q., & Helfand, D. J. 1991, ApJ, 370, 541

Wang, Q. D., Immler, S., & Pietsch, W. 1999, ApJ, 523, 121

Williams, R. M., & Chu, Y.-H. 1995, ApJ, 439, 132

Yang, H., Chu, Y.-H., Skillman, E. D., & Terlevich, R. 1996, AJ, 112, 146

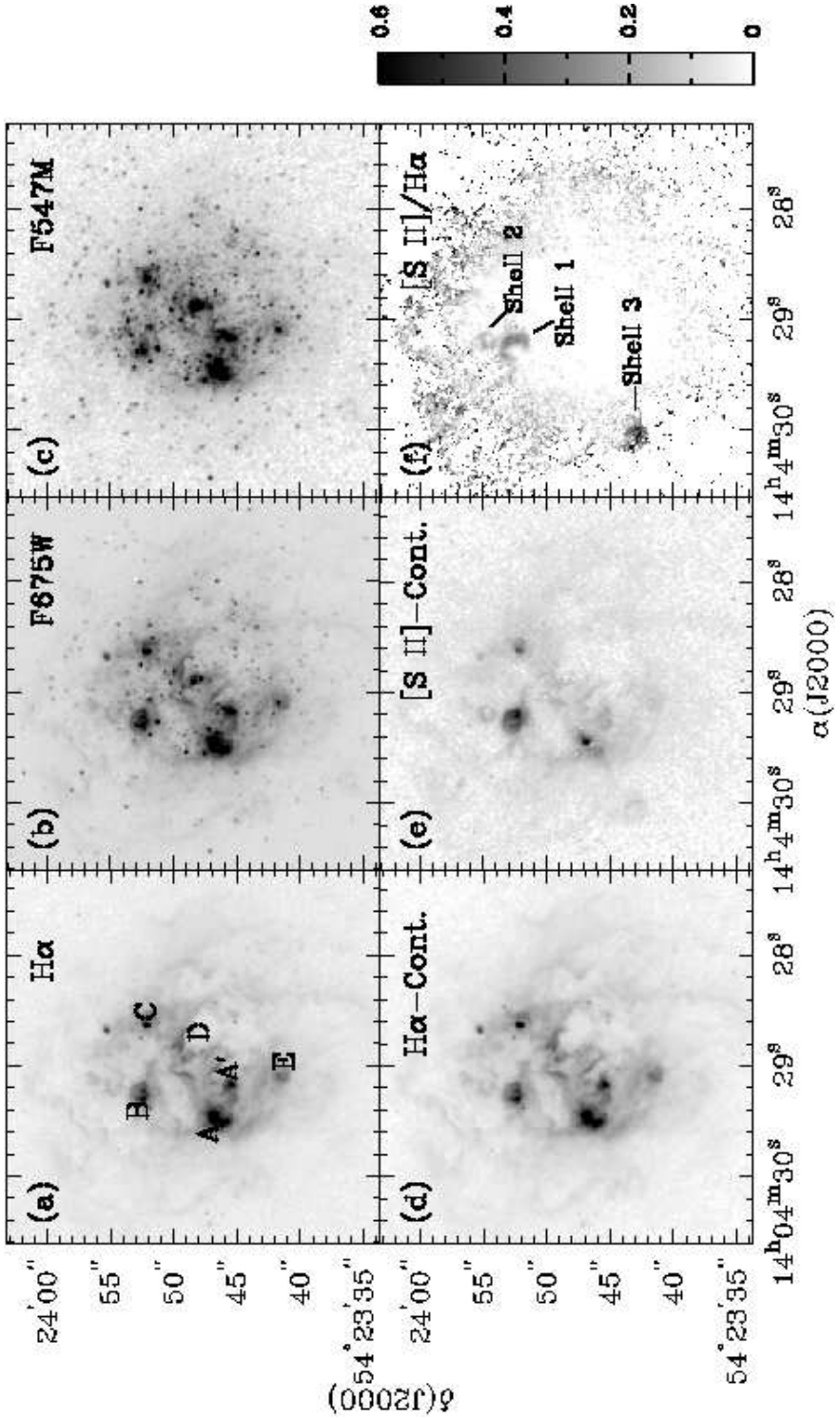

Fig. 1.— *HST* WFPC2 images of NGC 5471 in (a) Hα, (b) *F675W*, (c) *F547M*, (d) continuum-subtracted Hα, (e) continuum-subtracted [S II], and (f) [S II]/Hα. The grey-scale images in (a)–(e) are displayed with square-root image transfer functions. The [S II]/Hα ratio map in (f) is displayed with a linear image transfer function, as shown in the greyscale bar to its right.

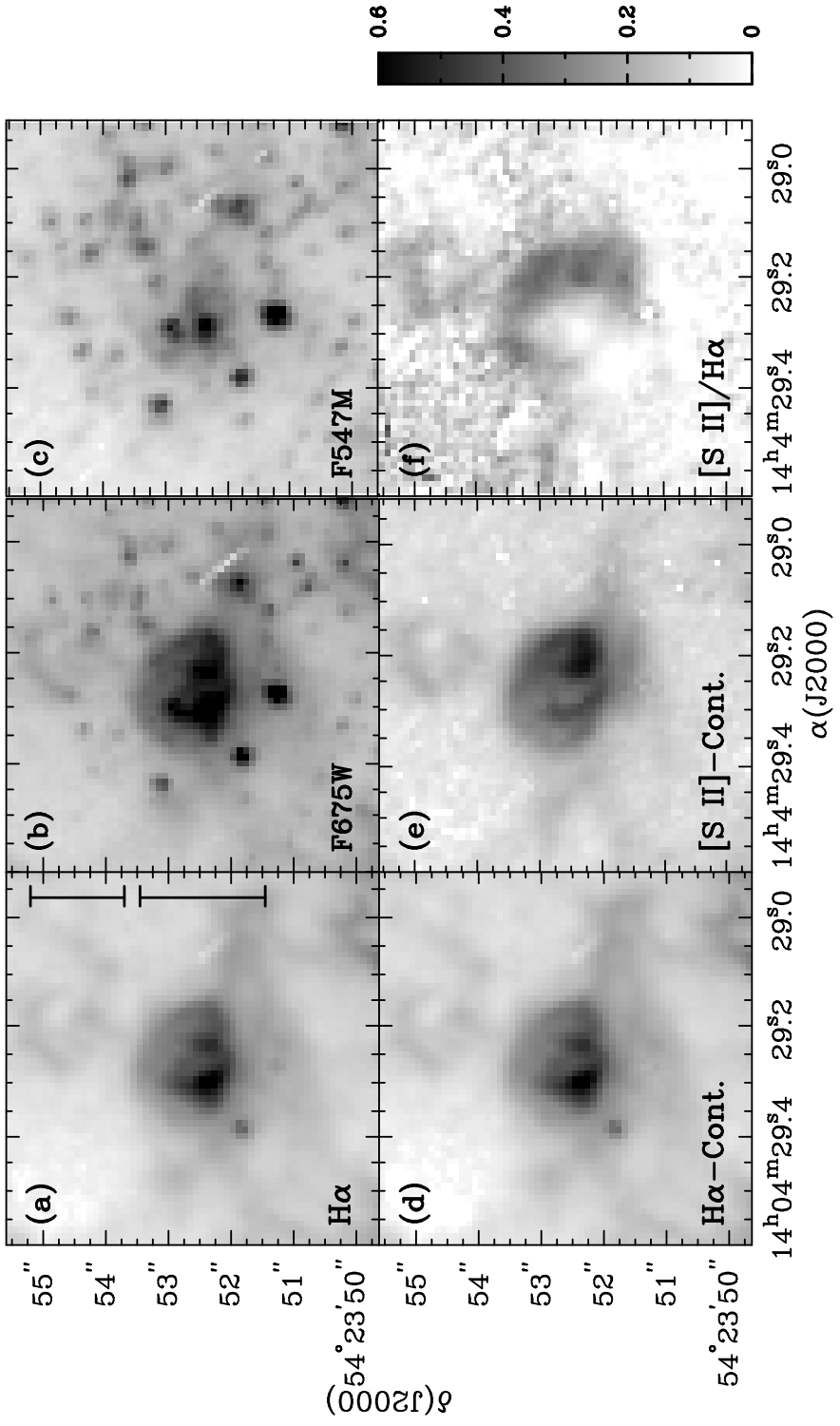

Fig. 2.— *HST* WFPC2 images of NGC 5471B in (a) Hα, (b) *F675W*, (c) *F547M*, (d) continuum-subtracted Hα, (e) continuum-subtracted [S II], and (f) [S II]/Hα. The grey-scale images in (a)–(e) are displayed with square-root image transfer functions. The [S II]/Hα ratio map in (f) is displayed with a linear image transfer function, as shown in the greyscale bar to its right. The lines in (a) mark the widths and locations of the E-W oriented slit of the echelle observations.

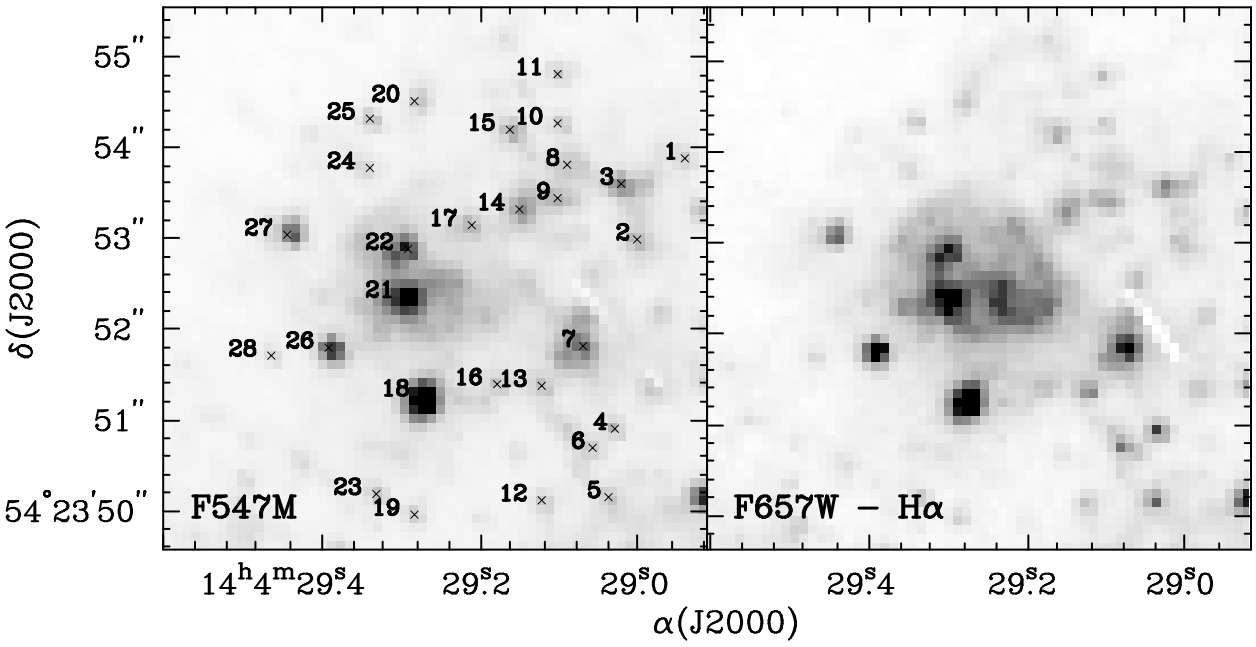

Fig. 3.— *HST* WFPC2 images of NGC 5471B in (a) *F547M* and (b) Hα-subtracted *F657W*. Stellar sources are identified and marked in (a)

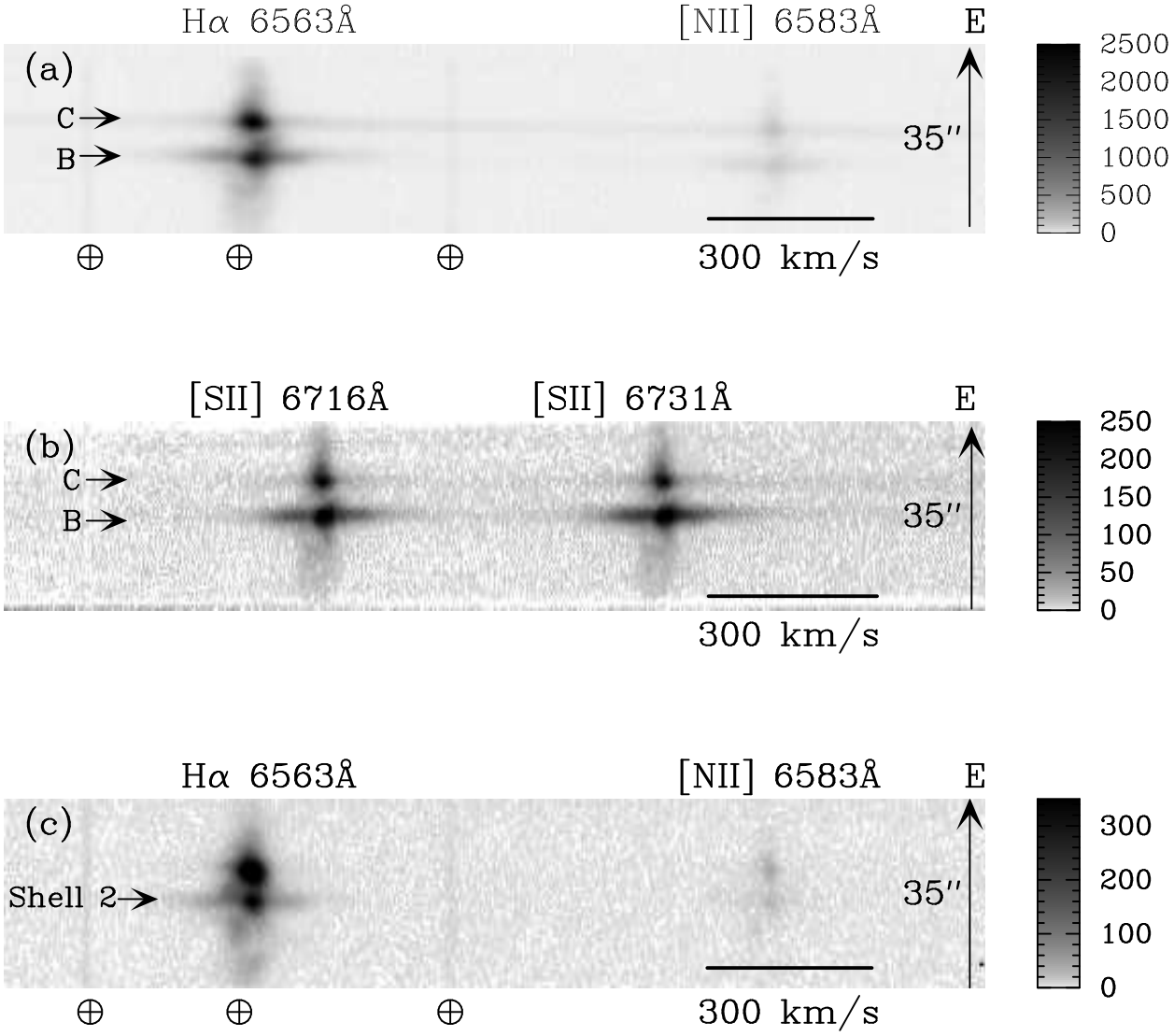

Fig. 4.— KPNO 4 m echellograms of (a) the Hα+[N II] λ6583 lines, and (b) the [S II] $\lambda\lambda$6716, 6731 lines along an E-W slit centered on NGC 5471B (=Shell 1), and (c) the Hα+[N II] λ6583 lines along an E-W slit centered on Shell 2. The C-component of NGC 5471, to the east of NGC 5471B, is also detected and marked in (a) and (b). The bright source to the east of Shell 2 is a bright compact H II region to the north of NGC 5471C. The images are displayed with square-root image transfer functions, as indicated by the greyscale bars on the right. The telluric lines marked by $\oplus$ are, from left to right, Hα λ6562.8, OH λ6568.8, and OH $\lambda\lambda$6577.2, 6577.4 lines. Both NGC 5471B and Shell 2 have an average heliocentric velocity of 297 ± 3 km s^{-1}.

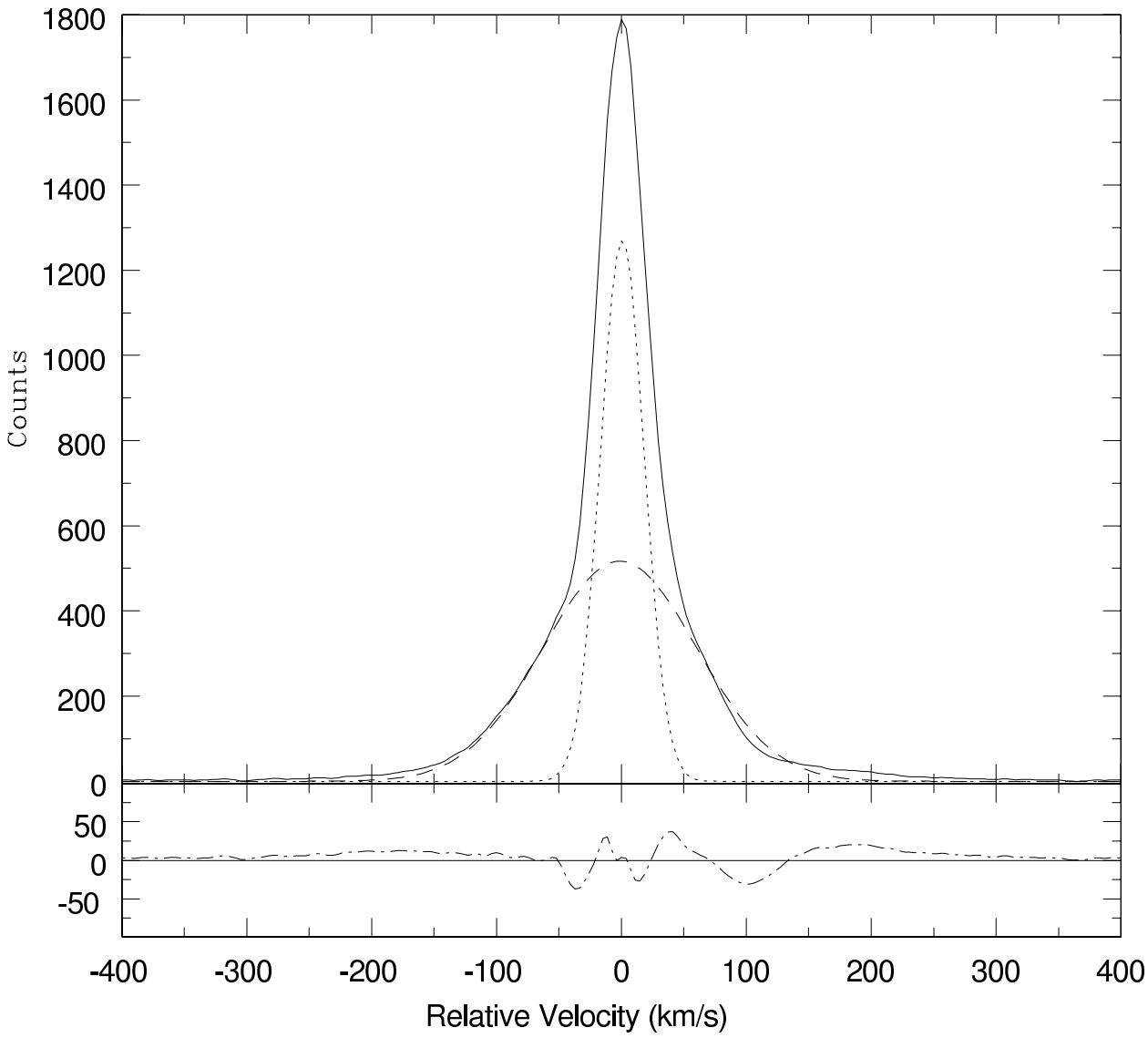

Fig. 5.— Hα velocity profile of NGC 5471B extracted from a $2''\times2\farcs9$ echelle aperture centered on NGC 5471B. The profile (in solid line) is fitted by two Gaussian components (in dotted and dashed lines). The residual of the fit, displayed in the lower panel, shows that high-velocity gas is detected over more than 600 km s^{-1}. The relative velocity in the horizontal axis is referenced to the heliocentric velocity of NGC 5471B, 297 km s^{-1}.

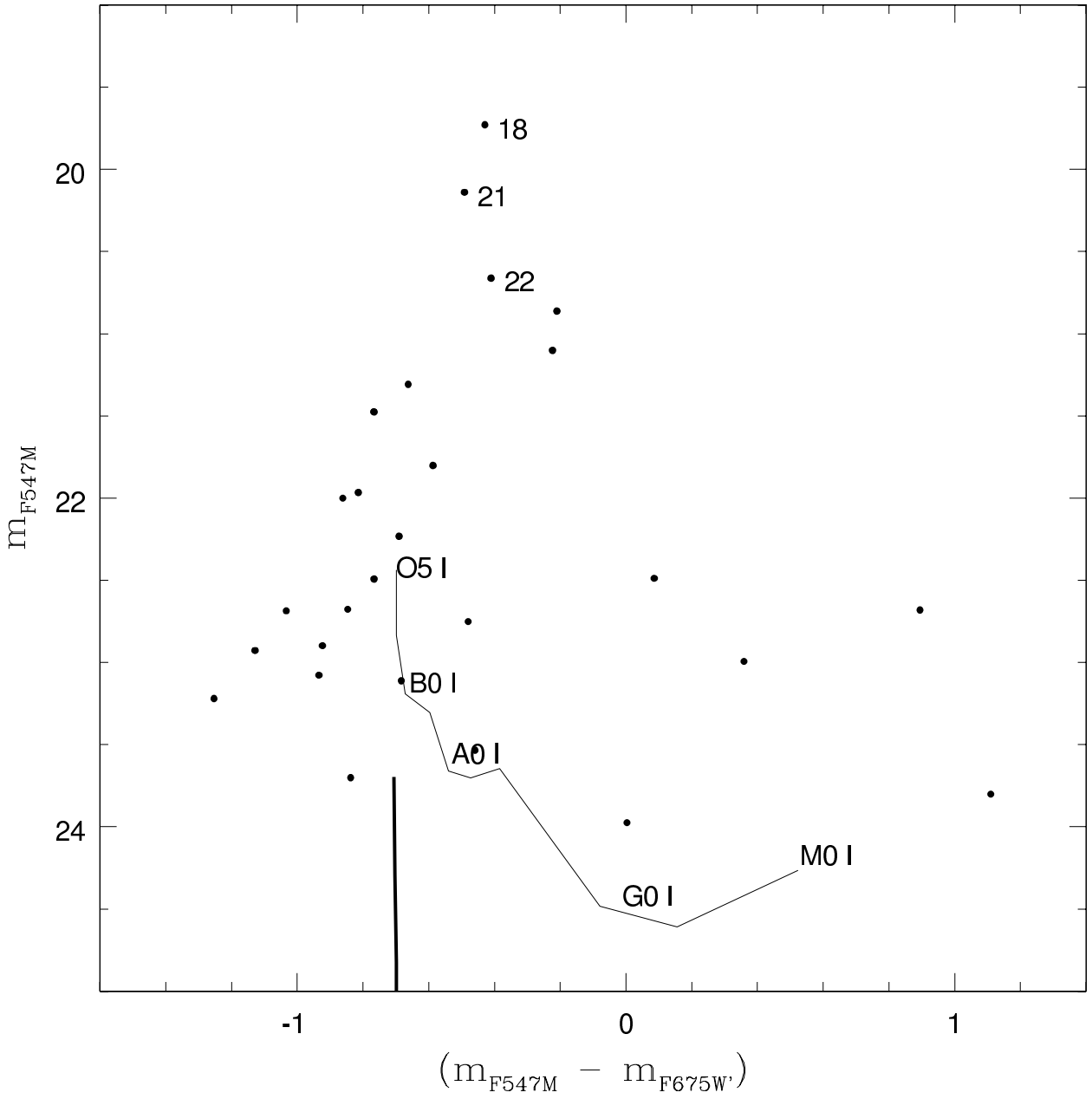

Fig. 6.— Color-magnitude diagram of the stellar sources in the vicinity of NGC 5471B. The stellar sources in Table 2 are plotted as •. The Hα-corrected *F675W* magnitude, $m_{F675W'}$, is used to reduce photometric errors caused by Hα contamination in the *F675W* band. Loci of the synthetic main sequence from O3 V downward are plotted in a thick line and the supergiants in a thin line, for a metallicity of 1/10 $Z_{\odot}$, a reddening of $E(B-V) = 0.16$ mag, and a distance modulus of 29.3 mag. The spectral types of the synthetic supergiants are marked.

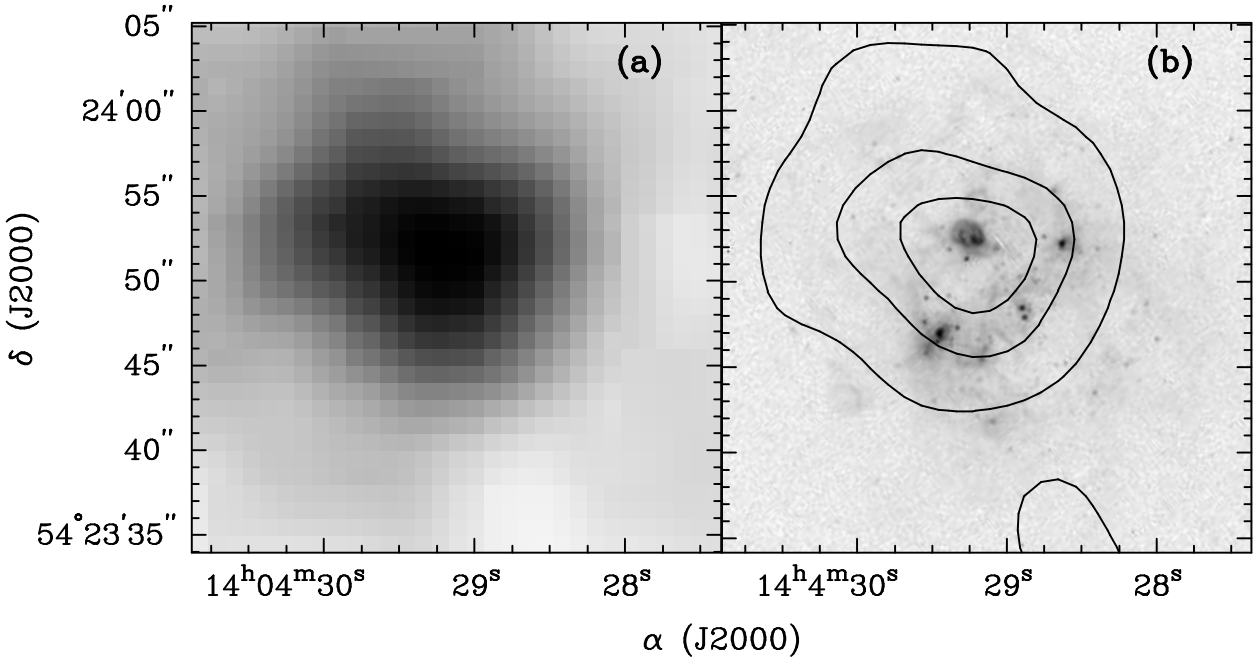

Fig. 7.— (a) *ROSAT* HRI image of NGC 5471. This HRI image is extracted from a 227 ks observation, and has been smoothed with a Gaussian of $\sigma = 3''$. (b) *HST* WFPC2 [S II] image overlaid with the HRI X-ray contours at levels of 25%, 50%, 75% and 90% of the peak value.

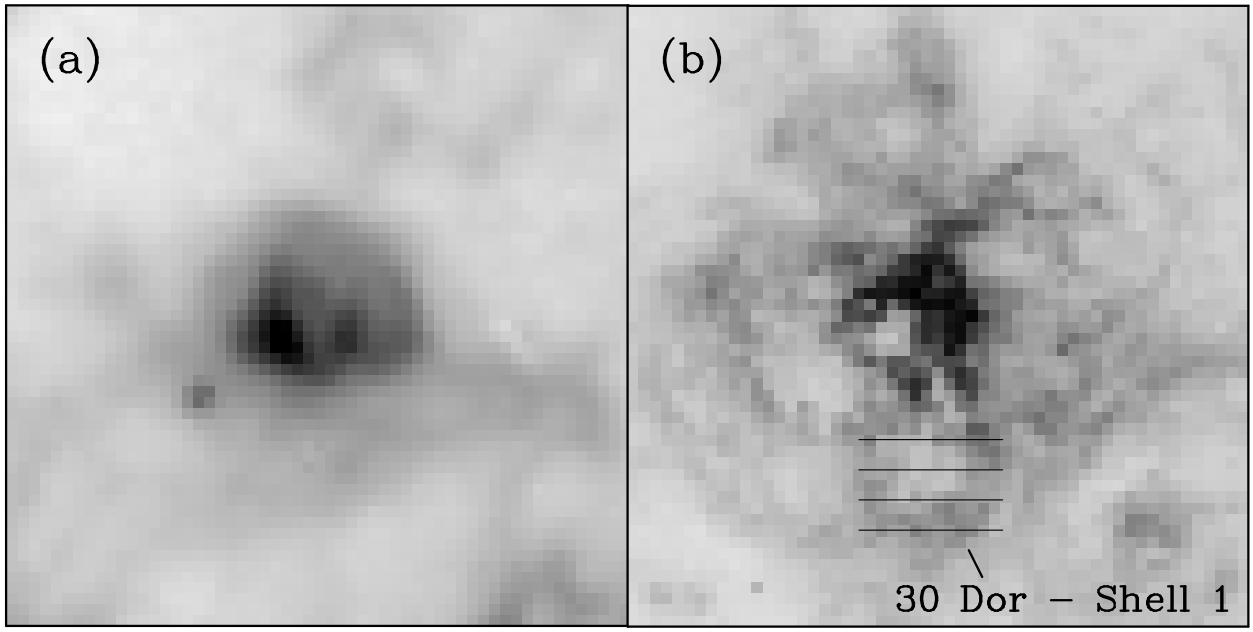

Fig. 8.— (a) *HST* WFPC2 Hα image of NGC 5471B. (b) Ground-based Hα image of 30 Dor binned to simulate a *HST* WFPC2 image of 30 dor at the distance of M101. Both images have a linear dimension of 200 pc × 200 pc, and are displayed with square-root image transfer functions. 30 Dor-Shell 1 and the echelle slit positions from Chu & Kennicutt (1994a) are marked over 30 Dor in (b).

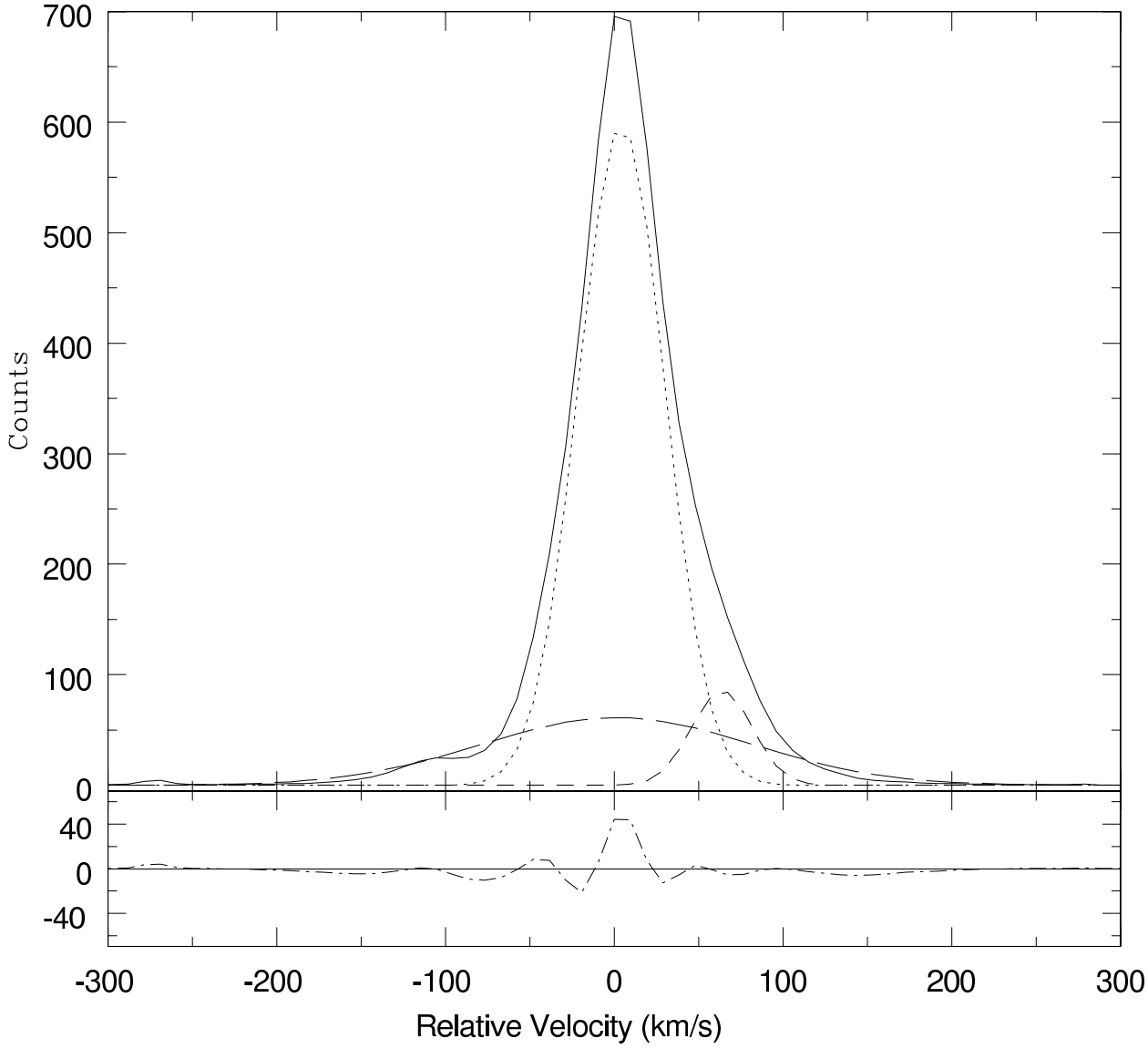

Fig. 9.— Pseudo-integrated Hα velocity profile of Shell 1 in 30 Dor. The profile (in solid line) is fitted by three Gaussian components (in dotted, short-dashed, and long-dashed lines). The residual of the fit is displayed in the lower panel. The relative velocity in the horizontal axis is referenced to the heliocentric velocity of 30 Dor, 275 km s^{-1}.

Table 1: Journal of *HST* WFPC2 Observations of NGC 5471

Filter	λ[a] (Å)	$\Delta\lambda$[a] (Å)	Band	Exposure (sec)	Image Root Name
F656N	6562	22	Hα	1×180	u4dn0305r
				2×600	u4dn0306r, u4dn0307r
F673N	6733	47	[S II]	3×700	u4dn0301r, u4dn0302r, u4dn0303r
F547M	5454	487	Strömgren y	2×100	u4dn030fr, u4dn030gr
				2×600	u4dn030dr, u4dn030er
F675W	6997	889	WFPC2 R	2×50	u4dn030ar, u4dn030br
				2×400	u4dn0308r, u4dn0309r

[a]The mean wavelengths (λ) and widths ($\Delta\lambda$) of the filters are taken from the WFPC2 Instrument Handbook (Biretta et al. 1996).

Table 2: Photometry of Stellar Sources in NGC 5471B

ID	R.A. (J2000)	Decl. (J2000)	m_{F547M} (mag)	m_{F675W} (mag)	$m_{F675W'}$[a] (mag)	$m_{F547M} - m_{F675W'}$ (mag)
1	14 04 28.94	54 23 53.9	22.68 ± 0.08	24.11 ± 0.25	23.52 ± 0.12	−0.85 ± 0.14
2	14 04 29.00	54 23 53.0	22.23 ± 0.10	23.15 ± 0.20	22.92 ± 0.13	−0.69 ± 0.16
3	14 04 29.02	54 23 53.6	21.48 ± 0.04	22.36 ± 0.05	22.24 ± 0.05	−0.77 ± 0.06
4	14 04 29.03	54 23 50.9	23.80 ± 0.47	23.58 ± 0.56	22.69 ± 0.11	1.11 ± 0.48
5	14 04 29.04	54 23 50.2	22.99 ± 0.21	21.91 ± 0.10	22.64 ± 0.10	0.36 ± 0.23
6	14 04 29.06	54 23 50.7	22.49 ± 0.10	22.49 ± 0.15	22.40 ± 0.08	0.09 ± 0.13
7	14 04 29.07	54 23 51.8	20.86 ± 0.03	20.88 ± 0.05	21.07 ± 0.03	−0.21 ± 0.05
8	14 04 29.09	54 23 53.8	21.97 ± 0.06	22.65 ± 0.08	22.78 ± 0.10	−0.81 ± 0.12
9	14 04 29.10	54 23 53.4	21.80 ± 0.07	22.51 ± 0.09	22.39 ± 0.08	−0.59 ± 0.10
10	14 04 29.10	54 23 54.3	23.08 ± 0.19	23.55 ± 0.23	24.01 ± 0.28	−0.93 ± 0.34
11	14 04 29.10	54 23 54.8	22.90 ± 0.09	24.62 ± 0.56	23.82 ± 0.17	−0.92 ± 0.20
12	14 04 29.12	54 23 50.1	23.53 ± 0.31	23.29 ± 0.32	23.99 ± 0.36	−0.46 ± 0.48
13	14 04 29.12	54 23 51.4	22.75 ± 0.18	23.71 ± 0.86	23.23 ± 0.36	−0.48 ± 0.41
14	14 04 29.15	54 23 53.3	21.47 ± 0.05	22.21 ± 0.09	22.24 ± 0.08	−0.77 ± 0.09
15	14 04 29.16	54 23 54.2	22.00 ± 0.05	22.71 ± 0.09	22.86 ± 0.08	−0.86 ± 0.09
16	14 04 29.18	54 23 51.4	23.97 ± 0.81	23.31 ± 0.85	23.97 ± 0.83	0.00 ± 1.16
17	14 04 29.21	54 23 53.1	22.68 ± 0.26	20.94 ± 0.08	21.79 ± 0.11	0.89 ± 0.28
18	14 04 29.27	54 23 51.3	19.73 ± 0.01	20.09 ± 0.02	20.16 ± 0.01	−0.43 ± 0.01
19	14 04 29.28	54 23 50.0	23.22 ± 0.11	24.24 ± 0.28	24.47 ± 0.25	−1.25 ± 0.27
20	14 04 29.28	54 23 54.5	22.49 ± 0.06	22.96 ± 0.16	23.26 ± 0.13	−0.77 ± 0.14
21	14 04 29.29	54 23 52.4	20.14 ± 0.02	19.66 ± 0.03	20.63 ± 0.04	−0.49 ± 0.05
22	14 04 29.29	54 23 52.9	20.66 ± 0.04	20.32 ± 0.07	21.07 ± 0.07	−0.41 ± 0.08
23	14 04 29.33	54 23 50.2	22.69 ± 0.07	23.82 ± 0.27	23.72 ± 0.14	−1.03 ± 0.16
24	14 04 29.34	54 23 53.8	23.11 ± 0.17	23.40 ± 0.21	23.79 ± 0.20	−0.68 ± 0.26
25	14 04 29.34	54 23 54.3	22.93 ± 0.10	24.05 ± 0.36	24.06 ± 0.23	−1.13 ± 0.25
26	14 04 29.39	54 23 51.8	21.10 ± 0.03	20.89 ± 0.03	21.32 ± 0.03	−0.22 ± 0.04
27	14 04 29.44	54 23 53.1	21.31 ± 0.03	21.84 ± 0.06	21.97 ± 0.04	−0.66 ± 0.05
28	14 04 29.46	54 23 51.7	23.70 ± 0.19	23.59 ± 0.24	24.54 ± 0.38	−0.84 ± 0.43

Note. — Units of right ascension are hours, minutes, and seconds, and units of declination are degrees, arminutes, and arcseconds.

[a]Apparent magnitudes measured from the Hα-subtracted *F675W* image of NGC 5471B.

Table 3: [S II]-Bright Shells in NGC 5471

Shell ID	R.A. (J2000)	Decl. (J2000)	Angular Size ($''$)	Linear Size[a] (pc)	Apparent [S II]/Hα	Corrected[b] [S II]/Hα
1	14 04 29.27	54 23 52.5	2.2 × 1.7	77 × 60	0.33 ± 0.03	0.5 ± 0.1
2	14 04 29.20	54 23 54.7	1.5 × 1.4	52 × 50	0.23 ± 0.03	0.5 ± 0.2
3	14 04 30.08	54 23 43.0	2.0 × 1.9	70 × 67	0.40 ± 0.05	0.8 ± 0.2

Note. — Units of right ascension are hours, minutes, and seconds, and units of declination are degrees, arminutes, and arcseconds.

[a]For a distance of 7.2 Mpc to M101 (Stetson et al. 1998).

[b]These corrected ratios are derived with an average background H II region emission subtracted.